



HAL
open science

Optimal optical conditions for Microalgal production in photobioreactors

Olivier Bernard, Liu-Di Lu

► **To cite this version:**

Olivier Bernard, Liu-Di Lu. Optimal optical conditions for Microalgal production in photobioreactors. Journal of Process Control, 2022, 112, pp.69-77. 10.1016/j.jprocont.2022.03.001 . hal-03323094v3

HAL Id: hal-03323094

<https://hal.science/hal-03323094v3>

Submitted on 30 Nov 2022

HAL is a multi-disciplinary open access archive for the deposit and dissemination of scientific research documents, whether they are published or not. The documents may come from teaching and research institutions in France or abroad, or from public or private research centers.

L'archive ouverte pluridisciplinaire **HAL**, est destinée au dépôt et à la diffusion de documents scientifiques de niveau recherche, publiés ou non, émanant des établissements d'enseignement et de recherche français ou étrangers, des laboratoires publics ou privés.

Optimal optical conditions for Microalgal production in photobioreactors

Olivier Bernard^{1,2}, Liu-Di Lu^{1,3,4}

¹*INRIA Sophia Antipolis Méditerranée, BIOCORE Project-Team, Université Nice Côte d'Azur, 2004, Route des Lucioles - BP 93, 06902 Sophia-Antipolis Cedex, France*

²*Sorbonne Université, INSU-CNRS, Laboratoire d'Océanographie de Villefranche, 181 Chemin du Lazaret, 06230 Villefranche-sur-mer, France*

³*INRIA Paris, ANGE Project-Team, 75589 Paris Cedex 12, France*

⁴*Sorbonne Université, CNRS, Laboratoire Jacques-Louis Lions, 75005 Paris, France*

Abstract

The potential of industrial applications for microalgae has motivated their recent fast development. Their growth dynamics depends on different factors that must be optimized. Since they get their energy from photosynthesis, light is a key factor that strongly influences their productivity. Light is absorbed and scattered in the liquid medium, and irradiance exponentially decreases towards the darkest part of the photobioreactor at a rate non-linearly depending on the biomass concentration. Maximizing productivity is then a tricky problem, especially when the growth rate is inhibited by an excess of light. Productivity optimization turns out to be highly dependent on how light is distributed along the reactor, and is therefore related to the extinction rate and the background turbidity. We propose a theoretical analysis of this problem, by introducing the concept of optical depth productivity for systems where background turbidity must be accounted for. A global optimum maximizing productivity is proposed, extending the concept of the compensation condition, consisting in compensating the algal growth rate at the bottom of the reactor by the respiration. This condition can drive the optimization of the surface biomass productivity depending on the minimum reachable depth. We develop a nonlinear controller and prove the global asymptotic stability of the biomass concentration towards the desired optimal value.

Keyword: Photobioreactor, Optimization, Nonlinear adaptive control, Microalgae, Light extinction, Compensation condition, Turbidostat.

1 Introduction

Microalgae are photosynthetic microorganisms whose potential has been highlighted in the last decades, especially for renewable energy and wastewater treatment [37, 18, 30]. Compared with terrestrial plants, whose growth is slower due to CO₂ availability, the high actual photosynthetic yield of microalgae cultures leads to higher biomass production potential. Some algal species can be grown to target numerous high added value commercial applications: pharmaceutical, cosmetics or food industries [12, 33]. These microorganisms are generally cultivated at industrial scale in simpler and cheaper open raceway ponds or in high-tech closed photobioreactors, using solar or artificial light depending on the applications.

The biomass productivity in these reactors depends on the photosynthesis efficiency resulting from the light distribution along depth. Light intensity is strongly attenuated in the photobioreactor due to the absorption and scattering of the microalgae and the background turbidity of the cultivation medium. Depending on the position of the algal cells in the reactor, they perceive different light intensities which further influence the photon harvesting dynamics. Light attenuation is generally described by a Beer-Lambert law [20] where the light extinction rate varies with the process type and algal concentration. Some studies have more accurately represented the way light is attenuated in the process, especially to deal with very dense multi-scattering medium where a photon can be scattered several times before being eventually absorbed [27]. There were a lot of works dedicated to better represent growth in a dense reactor [20, 36], with experimental validation [14, 19, 9] which were later carried out in more complicated geometries, also accounting for the influence of the solar angle [1, 29]. The influence of the background turbidity and the reactor geometry have often been neglected, even if its influence on the average growth rate turns out to be non-negligible, especially for some geometries [25].

The gap with industrial production is however still important and other factors should be taken into account, such as temperature, pH, nutrients, etc. There exists several realistic models for photobioreactor dynamics accounting for these effects [21, 5, 4, 32, 3]. These models were even made more accurate by including hydrodynamics [24, 11, 2]. Finally, a new generation of models is emerging when considering also the bacterial community interacting with microalgae [7, 31, 8]

Here we come back to the theory and focus on the core mechanisms involved in photobioreactor productivity, especially when background turbidity is taken into account. This theoretical study will give the main direction to be optimized in real systems. Authors in [26] provided an optimal condition to maximize the surface biomass productivity in a simplified framework. This so-called *compensation condition* consists in cancelling the net growth rate at the reactor bottom. It was validated by some experimental studies [34, 35]. This principle allows to adapt the biomass concentration to the reactor depth in order to maximize productivity. It has been assessed numerically, with Model Predictive Control, and shown to be still valid for more complicated and realistic cases

where temperature and light simultaneously vary [28, 10].

In this paper, we focus on understanding how this principle can be affected by the background turbidity, and more precisely how this can modify the theoretical results of [26]. Our first contribution, was to extend the work in [26] by choosing a more realistic description of the algal growth dealing with photoinhibition. Our second contribution consisted in considering a general biomass dependent light extinction function accounting for the background turbidity of the system. The concept of optical depth productivity is introduced, and a condition is derived on the optical depth for globally maximizing productivity. This optimum corresponds to the *compensation condition*. We then use this optimal condition to characterize the optimization of the surface biomass productivity depending on the minimum achievable water depth. When the light extinction rate is affine with respect to the algal biomass, an upper limit to the productivity (obtained for an infinitely small depth) is given. A nonlinear controller is given and is proved to stabilize the evolution of the biomass towards the optimal desired value. The optimal behaviours are illustrated in different cases by numerical experiments.

This paper is organized as follows. In Section 2, we define the key concepts such as average growth rate and light distribution. We then study the optimization problem in Section 3. More precisely we investigate the global behaviour of the optical depth productivity and the optimal condition in Subsection 3.1. The optimal biomass concentration for a given reactor depth to maximize the surface biomass productivity is investigated in Subsection 3.2. A nonlinear controller is then introduced in Section 4 to stabilize the biomass concentration towards its optimal value. We illustrate and discuss the behaviour of the optima in different cases by some numerical experiments in Section 5.

2 Description of the model

For a given light intensity I [$\mu\text{mol m}^{-2} \text{s}^{-1}$], the growth rate of microalgae is defined by a Haldane-type description parametrized as in [6]

$$\mu(I) := \mu_{\max} \frac{I}{I + \frac{\mu_{\max}}{\theta} \left(\frac{I}{I^*} - 1\right)^2}, \quad (1)$$

where θ is the initial slope of μ [d^{-1}], μ_{\max} denotes the maximum value of μ and I^* represents the optimal light intensity. This description results from a mechanical consideration of the light harvesting dynamics represented by the Han system in steady state [16]. The light attenuation is described by a Beer-Lambert law

$$I(X, z) := I_s \exp\left(\varepsilon(X)z\right), \quad (2)$$

where X [g m^{-3}] represents the biomass concentration, $z \in [-h, 0]$ denotes the vertical position of the algal cells with h [m] the depth and I_s is the light intensity at the reactor surface. The light extinction ε , which summarises the

light absorption and diffusion, is considered to be correlated to the biomass concentration X

$$\varepsilon(X) := \alpha_0(s)X^s + \alpha_1, \quad (3)$$

where $0 < s \leq 1$, $\alpha_0(s) > 0$ [$\text{m}^2 \text{g}^{-1}$] stands for the specific light extinction coefficient of the microalgae species. It depends on the parameter s . The background turbidity, α_1 [m^{-1}], is due to all non-microalgae components i.e. suspended solids and dissolved colored material. The dependence of s in α_0 will be omitted hereafter when no confusion may occur.

From (2) one can compute the mean light intensity received by the algae culture

$$\bar{I} = I_s \int_{-h}^0 e^{\varepsilon(X)z} dz = \frac{I_s}{\varepsilon(X)} \left(1 - e^{-\varepsilon(X)h}\right).$$

This quantity is a decreasing function of $\varepsilon(X)$, which confirms the intuition that a higher biomass concentration or a higher background turbidity leads to lower mean light received in the reactor, due to stronger light attenuation.

Replacing I by (2) in (1), one can see that the growth rate varies with depth of the reactor. Lower growth rate in the upper part of the reactor results from the photo-inhibition caused by the high light intensity. Similarly, growth rate is weak in the lower part of the reactor because of the low light intensity. The mean growth rate in the reactor is defined by

$$\bar{\mu}(X, h) := \frac{1}{h} \int_{-h}^0 \mu(I(X, z)) dz. \quad (4)$$

Applying then a change of the variable $y = \varepsilon(X)z$, it can be written as

$$\bar{\mu}(X, h) = \frac{1}{\varepsilon(X)h} \int_0^{\varepsilon(X)h} \mu(I(-y)) dy, \quad (5)$$

so that the mean growth rate depends on *the optical depth* $\varepsilon(X)h$. This quantity is denoted by Y [-] hereafter. In this case, the average growth rate (5) can also be written as a function of Y (i.e. $\bar{\mu}(X, h) = \bar{\mu}(Y)$). Our aim is to optimize the surface biomass productivity (units: $\text{g} \cdot \text{m}^{-2} \cdot \text{d}^{-1}$) which is defined by

$$\Pi := (\bar{\mu} - R)Xh. \quad (6)$$

Remark 2.1. *The evolution of the biomass concentration X is given by*

$$\dot{X} = (\bar{\mu} - R - D)X, \quad (7)$$

where R [d^{-1}] is the respiration rate and D [d^{-1}] denotes the reactor dilution rate. Note that at equilibrium, the biomass surface productivity Π is the product between dilution rate ($D = \bar{\mu} - R$) and surface biomass Xh .

Note that a nonlinear controller for D is introduced in Section 4 to stabilize (7) to the value of X optimizing productivity.

Remark 2.2. The average growth rate (4) is defined for flat reactors with a rectangular section. For more complex geometries, for instance horizontal triangular cylinder or horizontal semicircular cylinder, (4) still play an important role for the average growth rate in these reactors. We refer [25] for further details. For sake of simplicity, our analysis applies to flat systems (flat panels, raceways, ...) but could straightforwardly be extended to other shapes.

3 Analysis of the optimal productivity

In this section, we investigate the optimization problem associated with the productivity Π . Note that the biomass concentration X and the depth h are both defined in \mathbb{R}_+ .

3.1 Global optimality condition

First, let us define the optical depth productivity¹ (units: d^{-1}) by

$$P := (\bar{\mu} - R)Y. \quad (8)$$

Remark 3.1. According to the definition of the optical depth productivity (8), a thin reactor with high biomass concentration is equivalent to a deep reactor with low biomass concentration as long as they both share the same optical depth Y . A low value of Y means a weaker photon harvesting since less light is absorbed. On the reverse, a too high Y means that light hardly reaches the bottom of the reactor, with an area where respiration (loss of CO_2) exceeds growth (fixation of CO_2). Hence, it is necessary to determine the optimal Y value maximizing the efficiency of the productivity P .

Theorem 3.1. Given a surface light intensity I_s , there exists an optimum Y_{opt} which maximizes the optical productivity P . This value satisfies $\mu(I(Y_{\text{opt}})) = R$ and can be computed explicitly according to the growth rate at the surface $\mu(I_s)$:

$$Y_{\text{opt}} = \begin{cases} \ln \left(\frac{\frac{2I_s R \mu_{\max}}{\theta I_s^2}}{\mu_{\max} - R + \frac{2R\mu_{\max}}{\theta I_s^2} - \sqrt{(\mu_{\max} - R)(\mu_{\max} - R + \frac{4R\mu_{\max}}{\theta I_s^2})}} \right), & \mu(I_s) > R, \\ \ln \left(\frac{\frac{2I_s R \mu_{\max}}{\theta I_s^2}}{\mu_{\max} - R + \frac{2R\mu_{\max}}{\theta I_s^2} + \sqrt{(\mu_{\max} - R)(\mu_{\max} - R + \frac{4R\mu_{\max}}{\theta I_s^2})}} \right), & \mu(I_s) \leq R. \end{cases} \quad (9)$$

Proof. For a given Y , the optical productivity P can be written from (5) and (8)

$$\begin{aligned} P(Y) &= \int_0^{Y_{\text{opt}}} \mu(I(-y)) - R dy + \int_{Y_{\text{opt}}}^Y \mu(I(-y)) - R dy \\ &= P(Y_{\text{opt}}) + \int_{Y_{\text{opt}}}^Y \mu(I(-y)) - R dy, \end{aligned} \quad (10)$$

¹also called "optical productivity"

where Y_{opt} is chosen according to (9). On the other hand, for the function

$$\mu(I(-y)) = \frac{\mu_{\max} I(-y)}{I(-y) + \frac{\mu_{\max}}{\theta} \left(\frac{I(-y)}{I^*} - 1 \right)^2},$$

there exists a $y^* := \ln(I_s/I^*) > 0$ with $\mu(I(-y^*)) = \mu_{\max}$ such that $\mu(I(-y))$ is increasing from 0 to y^* and decreasing from y^* to $+\infty$. According to the value of $\mu(I(0))$ (i.e. $\mu(I_s)$), two cases must be considered:

- if $\mu(I(0)) = \mu(I_s) > R$, the second term of (10) is always negative. Indeed, in the case where Y is smaller than Y_{opt} , one finds $\mu(I(-y)) > R$, $\forall y < Y_{\text{opt}}$. In other words, the second term of (10) removes the microalgae which grow more than they respire. Otherwise, Y is greater than Y_{opt} , one finds $\mu(I(-y)) < R$, $\forall y > Y_{\text{opt}}$ (for the same reason as above). This means that the second term of (10) adds the microalgae which respire more than their growth.
- if $\mu(I(0)) = \mu(I_s) \leq R$, then there exists a $\tilde{y} \in [0, y^*)$ such that $\mu(I(-\tilde{y})) = R$. Then if Y is greater than \tilde{y} , the second term of (10) is negative for the same reason as above. Otherwise, the productivity $P(Y)$ is negative.

In both cases, the second term of (10) is negative. Thus Y_{opt} maximizes the quantity P .

In order to compute Y_{opt} , one needs to solve $\mu(I) = R$, or equivalently:

$$\frac{R\mu_{\max}}{\theta I^{*2}} I^2 + \left(R - \mu_{\max} - \frac{2R\mu_{\max}}{\theta I^*} \right) I + \frac{R\mu_{\max}}{\theta} = 0.$$

The discriminant of this second order polynomial equation is given by $\Delta = (\mu_{\max} - R)(\mu_{\max} - R + \frac{4R\mu_{\max}}{\theta I^*}) > 0$, which implies that there exists two real roots. The sum and the product of two roots are both positive, hence both of these two roots are also positive. Finally Y_{opt} can be determined by the growth rate at the surface $\mu(I_s)$:

- if $\mu(I_s) > R$, then there exists one root in the interval $(0, I_s)$ and one root in the interval $(I_s, +\infty)$. In this case, one has

$$Y_{\text{opt}} = \ln \left(\frac{\frac{2I_s R \mu_{\max}}{\theta I^{*2}}}{\mu_{\max} - R + \frac{2R\mu_{\max}}{\theta I^*} - \sqrt{(\mu_{\max} - R)(\mu_{\max} - R + \frac{4R\mu_{\max}}{\theta I^*})}} \right).$$

- if $\mu(I_s) \leq R$, then two roots both lie into the interval $(0, I_s]$. In this case, we choose the smaller one (since it represents the light at lower part of the reactors)

$$Y_{\text{opt}} = \ln \left(\frac{\frac{2I_s R \mu_{\max}}{\theta I^{*2}}}{\mu_{\max} - R + \frac{2R\mu_{\max}}{\theta I^*} + \sqrt{(\mu_{\max} - R)(\mu_{\max} - R + \frac{4R\mu_{\max}}{\theta I^*})}} \right).$$

This concludes the proof. \square

Remark 3.2. *As shown in (9), the value of Y_{opt} only depends on the model parameters $(\theta, \mu_{max}, I^*, R)$ and on the light intensity at the reactor surface I_s . In other words, the cancellation of the net growth rate at the bottom of the reactor is the optimal strategy to maximize optical depth productivity (see in Figure 2 for illustrations).*

3.2 Surface biomass productivity

In this section, we focus on the surface biomass productivity Π . From the definition of Π (6) and the definition of P (8), one has

$$\Pi = \frac{X}{\varepsilon(X)}P. \quad (11)$$

In general, it is not possible to apply the same strategy (as in the proof of Theorem 3.1) to optimize Π , since P and Π do generally not have the same behaviour. Only in the case where $s = 1$ and $\alpha_1 = 0$, the factor $\frac{X}{\varepsilon(X)}$ simplifies, leading to the same optimum. Using then Theorem 3.1, we deduce directly the following results.

Corollary 3.1. *If the light extinction function defined by (3) satisfies $\alpha_1 = 0$ and $s = 1$, then Y_{opt} defined by (9) maximizes the productivity Π and Y_{opt} is the global optimum. Moreover, $\tilde{Y}_{opt} := Y_{opt}/\alpha_0$ is the optimal surface biomass.*

Proof. Since $\alpha_1 = 0$ and $s = 1$, $Y = \varepsilon(X)h = \alpha_0\tilde{Y}$ with $\tilde{Y} := Xh$ the surface biomass. Meanwhile, using (11), one has $P(\cdot) = \alpha_0\Pi(\cdot)$, then following the same analysis, one finds that Y_{opt} maximizes $P(\cdot)$, therefore the productivity $\Pi(\cdot)$. Finally, \tilde{Y}_{opt} is given by Y_{opt}/α_0 . \square

Corollary 3.2. *If the objective is to reach a biomass concentration X_1 , there exists a unique reactor depth h_1 which satisfies $\varepsilon(X_1)h_1 = Y_{opt}$ and maximizes the productivity $\Pi(X_1, \cdot)$ for this target biomass.*

Proof. Since X_1 is fixed, then using (11), one has directly that the optimum is given by Y_{opt} . In this case, h_1 is defined by $Y_{opt}/\varepsilon(X_1)$. \square

In Corollary 3.2, we have studied the case with a fixed biomass concentration X . This result does not depend on the considered law $\varepsilon(X)$. However, optimizing X is more tricky, Corollary 3.1 provides a result in the case with a specific value of α_1 and s . In more general case, the strategy used in the proof of Theorem 3.1 may fail when optimizing X . Indeed, let (X_1, h_1) such that $Y_{opt} = \varepsilon(X_1)h_1$. For a biomass concentration $X > X_1$, one has $Y = \varepsilon(X)h_1 > Y_{opt}$. Applying then Theorem 3.1, one finds immediately $P(Y) < P(Y_{opt})$. However, in the case where the background turbidity is not negligible (i.e. $\alpha_1 > 0$), one has $\frac{X}{\varepsilon(X)} > \frac{X_1}{\varepsilon(X_1)}$ using the definition (3). Then according to (11), it is not clear if $\Pi(X_1, h_1)$ is larger than $\Pi(X, h_1)$. In this

way, we focus on the case where $\alpha_1 > 0$ in the following. Let us start with a technical lemma.

Lemma 3.1. *Let h_1 a given depth and (X_1, h_1) such that $Y_{\text{opt}} = \varepsilon(X_1)h_1$, then there exists $\tilde{X} > X_1$ such that $\Pi(\tilde{X}, h_1) > \Pi(X_1, h_1)$.*

Proof. Using the definition of the surface biomass productivity (6) and the definition of the average growth rate (4), and applying a change of variable $I = I_s \exp(\varepsilon(X)z)$, one has

$$\Pi(X, h_1) = \frac{X}{\varepsilon(X)} \int_{I(X, h_1)}^{I_s} \frac{\mu(I) - R}{I} dI.$$

Let us denote by $f(I) = \frac{\mu(I) - R}{I}$ and by $F(I)$ such that $F'(I) = f(I)$. Note that F can actually be found explicitly as shown in Appendix B. The latter equation then becomes $\Pi(X, h_1) = \frac{X}{\varepsilon(X)} (F(I_s) - F(I(X, h_1)))$. Taking the partial derivative with respect to X gives

$$\partial_X \Pi(X, h_1) = \frac{(1-s)\alpha_0 X^s + \alpha_1}{\varepsilon^2(X)} (F(I_s) - F(I(X, h_1))) - \frac{X}{\varepsilon(X)} f(I(X, h_1)) \partial_X I(X, h_1).$$

Since $Y_{\text{opt}} = \varepsilon(X_1)h_1$, using Theorem 3.1, one has immediately $\mu(I(X_1, h_1)) = \mu(I(Y_{\text{opt}})) = R$, then one finds $f(I(X_1, h_1)) = 0$. Moreover, $F(I_s) - F(I(X_1, h_1)) = P(Y_{\text{opt}}) > 0$ and $s \leq 1$. These imply that $\partial_X \Pi(X_1, h_1) > 0$. In other words, there exists $\tilde{X} > X_1$ such that $\Pi(\tilde{X}, h_1) > \Pi(X_1, h_1)$. This concludes the proof. \square

According to Corollary 3.2, the couple (X_1, h_1) satisfies $\varepsilon(X_1)h_1 = Y_{\text{opt}}$ and corresponds to the optimum of $\Pi(X_1, \cdot)$ for a given X_1 . However, the previous lemma implies that this is not the optimal condition to optimize $\Pi(\cdot, h_1)$ for a given h_1 . This then enables us to prove the next theorem.

Theorem 3.2. *If $\alpha_1 > 0$, there is no global optimum for the productivity $\Pi(\cdot, \cdot)$ in $\mathbb{R}_+ \times \mathbb{R}_+$.*

Proof. Let us assume that there exists a global optimum for the productivity Π denoted by (X^*, h^*) . Since (X^*, h^*) is a global optimum, in particular, this is an optimum in the direction of h . Using Corollary 3.2, we find $\varepsilon(X^*)h^* = Y_{\text{opt}}$. However, using Lemma 3.1, there exists $\tilde{X}^* > X^*$ such that $\Pi(\tilde{X}^*, h^*) > \Pi(X^*, h^*)$. This contradicts the fact that (X^*, h^*) is a global optimum. Therefore, the productivity $\Pi(\cdot, \cdot)$ has no global optimum. \square

Since no global optimum for the productivity Π can be found when $\alpha_1 > 0$, then we would like to study the asymptotic behaviour of Π . In the following, we focus on the optimum in the direction of X and in the direction of h separately. Given X_0 and consider the sequence $(X_n, h_n)_{n \in \mathbb{N}}$ defined by

$$h_n = \frac{Y_{\text{opt}}}{\varepsilon(X_{n-1})}, \quad X_n := \operatorname{argmax}_{X \in \mathbb{R}_+} \Pi(X, h_n). \quad (12)$$

From the definition above, the sequence $(X_{n-1}, h_n)_{n>0}$ corresponds to the optimum in the direction of h for X_{n-1} , whereas the sequence $(X_n, h_n)_{n>0}$ corresponds to the optimum in the direction of X for h_n . In plain words, these two sequences defined by (12) aims at searching the local optima by optimizing in the direction of h and in the direction of X alternately. Let us provide some more information about the sequence $(X_n, h_n)_{n>0}$.

Theorem 3.3. $\lim_{n \rightarrow \infty} X_n = \infty$, $\lim_{n \rightarrow \infty} h_n = 0$ and

$$\lim_{n \rightarrow \infty} \Pi(X_n, h_n) = \begin{cases} \frac{P(Y_{\text{opt}})}{\alpha_0}, & s = 1, \\ +\infty, & s < 1. \end{cases}$$

Proof. By Lemma 3.1, one has $(X_n)_{n \in \mathbb{N}}$ which is a strictly increasing sequence. Hence, the sequence $(h_n)_{n \in \mathbb{N}^*}$ is strictly decreasing by its construction (12). Since for each $n \in \mathbb{N}^*$, $h_n > 0$, then this sequence converges to a limit that we denote by h_{lim} . Assume that $h_{\text{lim}} > 0$, then from (12), one has

$$h_{\text{lim}} = \lim_{n \rightarrow \infty} h_n = \lim_{n \rightarrow \infty} \frac{Y_{\text{opt}}}{\varepsilon(X_{n-1})} = Y_{\text{opt}} \lim_{n \rightarrow \infty} \frac{1}{\alpha_0 X_{n-1} + \alpha_1},$$

which means that $\lim_{n \rightarrow \infty} X_n =: X_{\text{lim}} < \infty$. Then $(X_{\text{lim}}, h_{\text{lim}})$ is a global optimum, hence a contradiction with Theorem 3.2. Therefore $h_{\text{lim}} = 0$, which means that $X_{\text{lim}} = \infty$.

On the other hand, by the construction of these two sequences $(X_{n-1}, h_n)_{n>0}$, $(X_n, h_n)_{n>0}$ and Lemma 3.1, one has

$$\Pi(X_{n-1}, h_n) < \Pi(X_n, h_n) < \Pi(X_n, h_{n+1}).$$

Using (11), one has $\Pi(X_{n-1}, h_n) = \frac{X_{n-1}}{\varepsilon(X_{n-1})} P(Y_{\text{opt}})$ and $\Pi(X_n, h_{n+1}) = \frac{X_n}{\varepsilon(X_n)} P(Y_{\text{opt}})$. In the case $s = 1$, passing to the limit of the latter two equations gives

$$\lim_{n \rightarrow \infty} \Pi(X_{n-1}, h_n) = \lim_{n \rightarrow \infty} \frac{X_{n-1}}{\varepsilon(X_{n-1})} P(Y_{\text{opt}}) = P(Y_{\text{opt}}) \lim_{n \rightarrow \infty} \frac{X_{n-1}}{\alpha_0 X_{n-1} + \alpha_1} = \frac{P(Y_{\text{opt}})}{\alpha_0},$$

$$\lim_{n \rightarrow \infty} \Pi(X_n, h_{n+1}) = \lim_{n \rightarrow \infty} \frac{X_n}{\varepsilon(X_n)} P(Y_{\text{opt}}) = P(Y_{\text{opt}}) \lim_{n \rightarrow \infty} \frac{X_n}{\alpha_0 X_n + \alpha_1} = \frac{P(Y_{\text{opt}})}{\alpha_0}.$$

This gives $\lim_{n \rightarrow \infty} \Pi(X_n, h_n) = \frac{P(Y_{\text{opt}})}{\alpha_0}$. However, in the case $0 < s < 1$, the previous limits become

$$\lim_{n \rightarrow \infty} \Pi(X_{n-1}, h_n) = \lim_{n \rightarrow \infty} \frac{X_{n-1}}{\varepsilon(X_{n-1})} P(Y_{\text{opt}}) = \frac{P(Y_{\text{opt}})}{\alpha_0} \lim_{n \rightarrow \infty} X_{n-1}^{1-s} = +\infty,$$

$$\lim_{n \rightarrow \infty} \Pi(X_n, h_{n+1}) = \lim_{n \rightarrow \infty} \frac{X_n}{\varepsilon(X_n)} P(Y_{\text{opt}}) = \frac{P(Y_{\text{opt}})}{\alpha_0} \lim_{n \rightarrow \infty} X_n^{1-s} = +\infty.$$

Therefore, $\lim_{n \rightarrow \infty} \Pi(X_n, h_n) = +\infty$. This concludes the proof. \square

Corollary 3.3. For $s = 1$, the sequence (X_n, h_n) verifies $\lim_{n \rightarrow \infty} \varepsilon(X_n) h_n = Y_{\text{opt}}$, and the growth rate at the reactor bottom satisfies $\lim_{n \rightarrow \infty} \mu(I(X_n, h_n)) = R$.

Proof. By the construction of sequences $(X_{n-1}, h_n)_{n>0}$, $(X_n, h_n)_{n>0}$ and Lemma 3.1, one has

$$\Pi(X_{n-1}, h_n) < \Pi(X_n, h_n) < \Pi(X_n, h_{n+1}).$$

Using (11), the previous inequalities become

$$\frac{X_{n-1}}{\varepsilon(X_{n-1})} P(Y_{\text{opt}}) < \frac{X_n}{\varepsilon(X_n)} P(\varepsilon(X_n)h_n) < \frac{X_n}{\varepsilon(X_n)} P(Y_{\text{opt}}),$$

where we use the fact that $\varepsilon(X_{n-1})h_n = \varepsilon(X_n)h_{n+1}Y_{\text{opt}}$ by Definition (12). Since $\frac{X_n}{\varepsilon(X_n)} > 0$, dividing the latter inequalities by $\frac{X_n}{\varepsilon(X_n)} > 0$ gives

$$\frac{\varepsilon(X_n)X_{n-1}}{\varepsilon(X_{n-1})X_n} P(Y_{\text{opt}}) < P(\varepsilon(X_n)h_n) < P(Y_{\text{opt}}).$$

Moreover, using the definition (3) for $s = 1$, one has

$$\frac{\varepsilon(X_n)X_{n-1}}{\varepsilon(X_{n-1})X_n} = \frac{\alpha_0 X_n X_{n-1} + \alpha_1 X_{n-1}}{\alpha_0 X_n X_{n-1} + \alpha_1 X_n} > 1 - \frac{\alpha_1}{\alpha_0 X_{n-1} + \alpha_1}.$$

In other words,

$$\left(1 - \frac{\alpha_1}{\alpha_0 X_{n-1} + \alpha_1}\right) P(Y_{\text{opt}}) < P(\varepsilon(X_n)h_n) < P(Y_{\text{opt}}).$$

Denoting by $Y_n = \varepsilon(X_n)h_n$ and passing the latter inequalities to the limit, one then has $\lim_{n \rightarrow \infty} P(Y_n) = P(Y_{\text{opt}})$. On the other hand, $P(Y) = \int_0^Y \mu(I(-y)) - R dy$ is decreasing on the interval $(Y_{\text{opt}}, +\infty)$ for the reason that $\mu(I(-y))$ is decreasing and $\mu(I(-y)) < R$ on this interval. Since for all $n \in \mathbb{N}$, $Y_n > Y_{\text{opt}}$, one has $\lim_{n \rightarrow \infty} Y_n = Y_{\text{opt}}$. Finally $\mu(I(-y))$ is a continuous function with respect to y in \mathbb{R}_+ , one has

$$\lim_{n \rightarrow \infty} \mu(I(X_n, h_n)) = \lim_{n \rightarrow \infty} \mu(I(Y_n)) = \mu(I(Y_{\text{opt}})) = R.$$

This concludes the proof. \square

The previous theorem shows that without constraint on the reactors, an infinite thin reactor with an infinite dense biomass concentration can maximize the productivity. According to how light attenuates in the reactors (i.e. value of s), this productivity can be increased infinitely. However for real reactors, there is a constraint on the minimal reactor depth h_{lim} (below which mixing is no more possible). An optimal solution can then be found in this case. Indeed, as shown in Theorem 3.3, a higher productivity can be obtained for higher biomass concentration and smaller reactor depth. Considering the minimal reactor depth, one can find the optimal biomass concentration maximizing the productivity.

4 Optimal control implementation in closed loop

As shown in previous section, there exists optimal biomass concentration for a given reactor depth h . In this section, let us show that the evolution of the biomass concentration X (defined in (7)) can be stabilized to a desired biomass concentration by applying an appropriate controller. More precisely, we consider the dilution rate D in (7) as a controller. Let us denote by $X^* \in (0, X(0))$ the desired biomass concentration.

Assumption 1 (H1). *We assume that:*

- a. *thanks to an oxygen probe, the quantity $\Phi := (\bar{\mu}(X, h) - R)X$ is measured on-line from the plant,*
- b. *the growth rate for the influent light intensity is larger than the respiration (i.e. $\mu(I_s) > R$),*
- c. *the maximal dilution rate D_{\max} is larger than the maximal growth rate μ_{\max} .*

The quantity Φ denotes the average oxygen production which is available from the reactor. Indeed, oxygen sensors are currently available and easy to implement. Note that numerical estimators can also be applied to obtain the quantity Φ . The influent light intensity is logically assumed to enable biomass growth, i.e. to be neither too low nor too inhibiting. The dilution rate (by medium addition in the system) and harvesting rate is adapted to the maximal growth rate of the species.

Proposition 4.1. *The control law*

$$D = \begin{cases} D_{\max} & X \geq \bar{X} \\ (\bar{\mu}(X, h) - R) \frac{X}{X^*} & X < \bar{X} \end{cases} \quad (13)$$

globally stabilizes equation (7) towards the positive point X^ .*

Remark 4.1. $\bar{X} > X^*$ is chosen to determine the area where the control will be at its maximum rate. It is defined so that $(\mu_{\max} - R) \frac{\bar{X}}{X^*} < D_{\max}$.

Proof. From the definition of (13), the control variable D is positive. On the other hand, $\bar{\mu}(0, h) > R$, $\lim_{X \rightarrow \infty} \bar{\mu}(X, h) = 0$ and $\bar{\mu}(\cdot, h)$ is continuously decreasing with respect to X . If the initial state $X(0) \geq \bar{X}$, then replacing $D = D_{\max}$ into (7) gives

$$\dot{X} = (\bar{\mu}(X, h) - R - D_{\max})X.$$

In particular, $\bar{\mu}(X(0), h) - R - D_{\max} < 0$, hence there exists a time $t_1 > 0$ such that the state X decreases from 0 to t_1 and $X(t_1) = \bar{X}$. When $t > t_1$, $D = \frac{\Phi}{X^*}$. Replacing $D = \frac{\Phi}{X^*}$ into (7) gives

$$\dot{X} = (\bar{\mu}(X, h) - R) \frac{X}{X^*} (X^* - X) = \frac{\Phi}{X^*} (X^* - X). \quad (14)$$

Note that the system is now in the positive invariant region $X < \bar{X}$ and cannot come back again to $X \geq \bar{X}$. Moreover, $0 < \bar{\mu}(X, h) - R < \mu_{\max} - R$. Then, integrating (14) gives $\forall t \geq t_1, \quad 0 < X^* \leq X(t) \leq X(0)$.

In the case the initial state $X(0) \in (0, \bar{X})$, the control variable $D = \frac{\Phi}{X^*}$ and the evolution equation (7) once again becomes (14), hence we follow the small strategy as above.

Finally we find in both two cases that

$$\forall t \geq 0, \quad 0 < X^* \leq X(t) \leq X(0).$$

Therefore, the state X^* is globally exponentially stable for the evolution equation (7) by using the control law (13). \square

5 Numerical results

In this section, we will illustrate some optimal conditions to maximize the algal productivity. In this way, we first introduce an algorithm to compute the sequences defined in (12). We then give the parameters that we use for the numerical experiments and show some numerical results.

5.1 Numerical algorithm

In practice, one can use the next algorithm to compute for two sequences $(X_{n-1}, h_n)_{n>0}$ and $(X_n, h_n)_{n>0}$ defined by (12).

Algorithm 1 Search Optimum

- 1: **Input:** $Y_{\text{opt}}, n_{\text{max}}$ and X_0 .
 - 2: **Output:** $(X_n, h_n)_{n>0}$
 - 3: Set $n := 0$.
 - 4: **while** $n < n_{\text{max}}$ **do**
 - 5: Set $n = n + 1$.
 - 6: Compute $h_n = Y_{\text{opt}}/\varepsilon(X_{n-1})$.
 - 7: Compute X_n such that $d\Pi_X(X_n, h_n) = 0$.
 - 8: **end while**
-

5.2 Parameter settings

The Han model parameters are taken from [13] and recalled in Table 1. Parameters $\mu_{\max} = 1.64 \text{ d}^{-1}$, $\theta = 4.09 \times 10^{-7}$ and $I^* = 202.93 \mu\text{mol m}^{-2} \text{ s}^{-1}$ are then derived from equation (20). The considered surface light intensity is $I_s = 2000 \mu\text{mol m}^{-2} \text{ s}^{-1}$. For $s = 1$, we take from [25] the specific light extinction coefficient for the species *Chlorella pyrenoidosa* $\alpha_0 = 0.2 \text{ m}^2 \text{ g}^{-1}$ and the background turbidity $\alpha_1 = 10 \text{ m}^{-1}$. Note that for the case where $s < 1$,

Table 1: Parameter values for Han Model.

k_r	$6.8 \cdot 10^{-3}$	s^{-1}
k_d	$2.99 \cdot 10^{-4}$	-
τ	0.25	s
σ_H	0.047	$m^2 \mu mol^{-1}$
k_H	$8.7 \cdot 10^{-6}$	-
R	$1.389 \cdot 10^{-7}$	s^{-1}

we compute the coefficient $\alpha_0(s)$ to find the one providing an extinction coefficient as close as possible to the reference linear case which is generally the one measured:

$$\alpha_0(s) := \operatorname{argmin}_{X \in [X_{\min}, X_{\max}]} |\alpha_0(1)X - \alpha_0(s)X^s|. \quad (15)$$

5.3 Numerical study

In this section, we provide some numerical tests to illustrate the influence of the water depth h , the biomass concentration X and the light extinction function $\varepsilon(X)$ on algal productivity.

5.3.1 Evaluation of different light extinction coefficient

As mentioned in the previous section, the light extinction coefficient α_0 needs to be better estimated when $s < 1$, in comparison with the reference case $s = 1$. For this reason, for a range of biomass concentration X in $[0, 1000]$ ($g \cdot m^{-3}$), we use (15) to find α_0 that provide the same average extinction rate. Figure 1 shows $\varepsilon(X)$ defined by (3) for different values of s when the background turbidity $\alpha_1 > 0$.

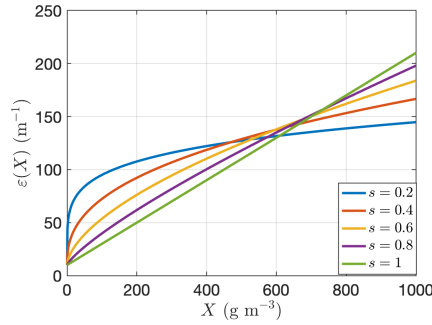


Figure 1: $\varepsilon(X)$ with respect to X for $s \in \{0.2, 0.4, 0.6, 0.8, 1\}$.

5.3.2 Global optimum of optical depth

The optimal optical depth Y_{opt} can be computed explicitly using (9) once the light intensity at the reactor surface I_s and the model parameters $(\theta, \mu_{\max}, I^*, R)$ are fixed. Figure 2 presents the evolution of the growth rate μ and optical depth productivity P with respect to y for different value of s and α_1 . One

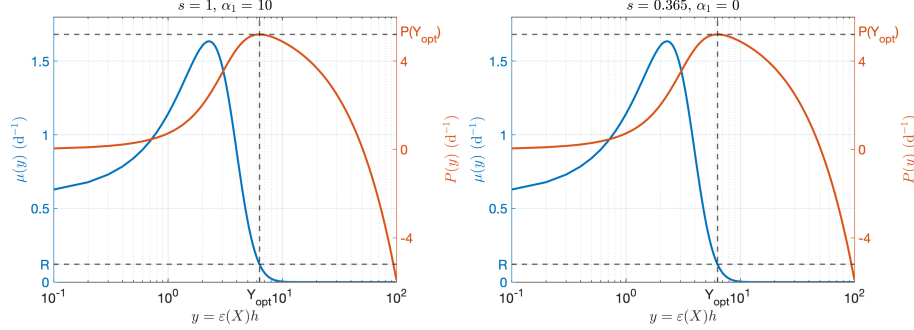


Figure 2: Growth rate μ and optical depth productivity P with respect to y . Left: $s = 1$ and $\alpha_1 = 10 \text{ m}^{-1}$. Right: $s = 0.365$ and $\alpha_1 = 0 \text{ m}^{-1}$.

can see that the optimum is obtained with $Y_{\text{opt}} = 6.337$, which also satisfies numerically $\mu(I(Y_{\text{opt}})) = R$. Moreover, as mentioned in Remark 3.2, Y_{opt} does not change for other values of α_1 and s .

In the same way, for a given biomass concentration X , Corollary 3.2 provides a condition to determine the optimal depth to maximize the surface biomass productivity Π . Figure 3 illustrates this corollary with a biomass concentration $X = 50 \text{ g} \cdot \text{m}^{-3}$ for different values of s and α_1 . Note that the optimal depth

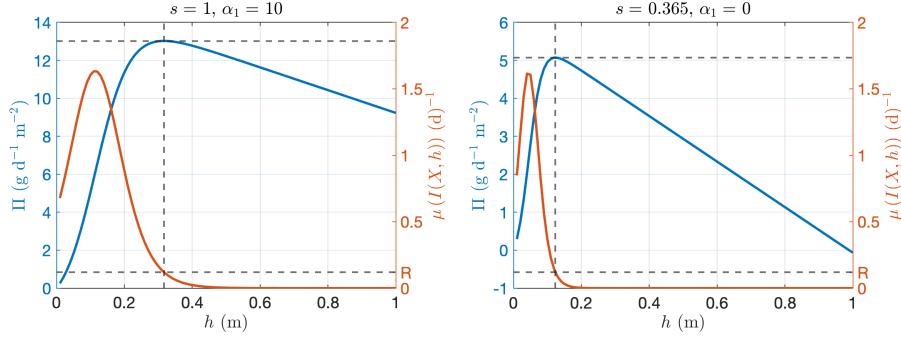


Figure 3: Productivity (Π) and net growth rate ($\mu_{\text{net}}(X, h)$) with respect to depth (h) for $X = 50 \text{ g} \cdot \text{m}^{-3}$. Left: $s = 1$ and $\alpha_1 = 10 \text{ m}^{-1}$. Right: $s = 0.365$ and $\alpha_1 = 0 \text{ m}^{-1}$.

h^* satisfies the relation $\varepsilon(X)h^* = Y_{\text{opt}}$. In other words, one can see that this optimum satisfies $\mu(I(X, h^*)) = R$. It is worth remarking that the range of the

productivity Π changes for different value of s and α_1 , this motivates the next test, where we study how these parameters affect algal growth.

5.3.3 Influence of the background turbidity and s

Here we study the influence of the background turbidity α_1 and the value of s on the productivity Π . We keep the biomass concentration value $X = 50 \text{ g} \cdot \text{m}^{-3}$ and compute h by using the relation $\varepsilon(X)h = Y_{\text{opt}}$ for different values of α_1 and s . Note that the depth h computed in this way is the optimum to maximize the productivity for the given biomass concentration. Figure 4 represents the optimal surface biomass productivity Π with respect to the background turbidity. As we can expect intuitively, the larger the background turbidity is, the smaller

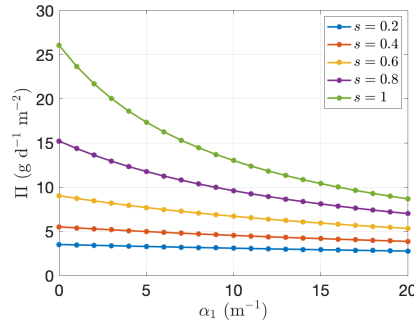


Figure 4: Optimal surface biomass productivity with respect to the background turbidity α_1 for $X = 50 \text{ g} \cdot \text{m}^{-3}$ and different value of s .

the productivity is. Furthermore, the productivity increases with the value of s for a fixed value of turbidity α_1 .

5.3.4 Local optimum in the case $s = 1$

In reality, the depth h depends on the type of reactors. As an example, $h = 0.1 \text{ m} - 0.5 \text{ m}$ for raceway ponds, $h = 1 \text{ cm} - 10 \text{ cm}$ for tubular photobioreactors and $h = 0.1 \text{ mm} - 1 \text{ mm}$ for biofilm reactors (where the microalgal biomass is fixed on a support). By knowing the lowest bound admissible for the reactor depth (depending on the process type), we only need to optimize the productivity in the direction of X . Note that the turbidity α_1 may change the optimal condition to maximize the surface biomass productivity Π . Indeed, Figure 5 illustrates this for a reactor depth $h = 0.15 \text{ m}$. Note that X_0 satisfies the relation $\varepsilon(X_0)h = Y_{\text{opt}}$ which also means that the net growth rate at the bottom of the reactor is zero (see the blue point in these two figures). On the other hand, the red point (X_1, h) is the optimum which maximize the surface biomass productivity Π for this given depth h . One can see that $X_0 = X_1 = 158.427 \text{ g} \cdot \text{m}^{-3}$ in the case the background turbidity is zero in the system (Left), meaning that the optimum is the point which cancels the net average growth rate at the reactor bottom as we have mentioned in Corollary 3.1.

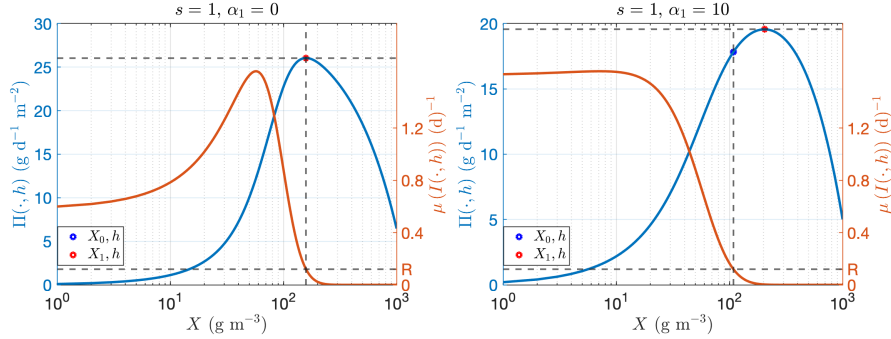


Figure 5: Productivity (Π) with respect to biomass concentration (X) for $h = 0.15$ m. Left: $\alpha_1 = 0 \text{ m}^{-1}$. Right: $\alpha_1 = 10 \text{ m}^{-1}$.

However, Lemma 3.1 indicates that by taking into account the background turbidity (Right), these two points are no longer the same and the optimum then satisfies $X_1 = 204.190 \text{ g} \cdot \text{m}^{-3} > X_0 = 108.427 \text{ g} \cdot \text{m}^{-3}$.

The global behaviour of the surface biomass productivity Π is represented on Figure 6, for $h \in (0, 1]$ and $X \in (0, 1000]$. To discuss the influence of the background turbidity, we consider two possible values, $\alpha_1 = 0 \text{ m}^{-1}$ and $\alpha_1 = 10 \text{ m}^{-1}$. Note that the blue points in the left figure (X, h) satisfy the relation

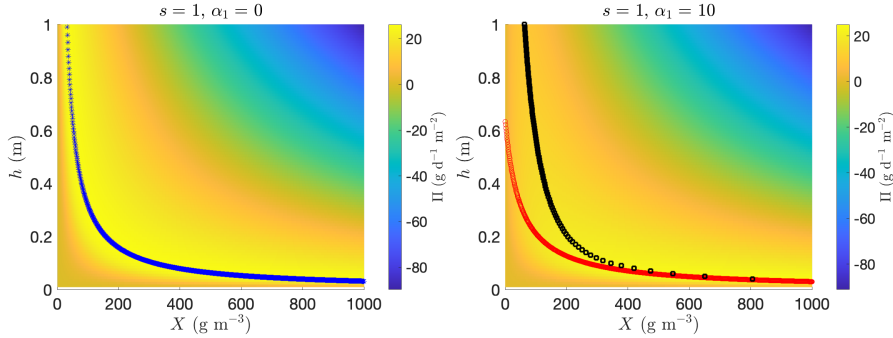


Figure 6: Global behaviour of productivity (Π) with respect to depth (h) and biomass concentration (X). Left: $\alpha_1 = 0 \text{ m}^{-1}$. The blue stars represent the optimal couple (X, h) such that Π finds its global maximum. Right: $\alpha_1 = 10 \text{ m}^{-1}$. The red circles represent the suboptimal couple (X, h) where Π finds its maximum in the direction of h for a given X . The black squares represent the suboptimal couple (X, h) where Π finds its maximum in the direction of X for a given h .

$\varepsilon(X)h = Y_{\text{opt}}$ which is also the global optimum. However, by taking into account the background turbidity (see figure on the right), no global optimum exists as mentioned in Theorem 3.2. Instead, for a given biomass concentration, the

optimal depths can still be found using the relation $\varepsilon(X)h = Y_{\text{opt}}$ (represented by the red circles in the right figure). For a given water depth, the optimal concentrations are obtained by cancelling the derivative of $\Pi(\cdot, h)$ (represented by the black squares in the right figure). Furthermore, one can observe that this two suboptima become closer when X increases and h decreases, meanwhile the productivity also increases in this direction.

Let us set $X_0 = 50 \text{ g} \cdot \text{m}^{-3}$, $\alpha_1 = 10 \text{ m}^{-1}$ and $n_{\text{max}} = 10^4$. Figure 7 illustrates the properties of these two sequences constructed by Algorithm 1. Starting

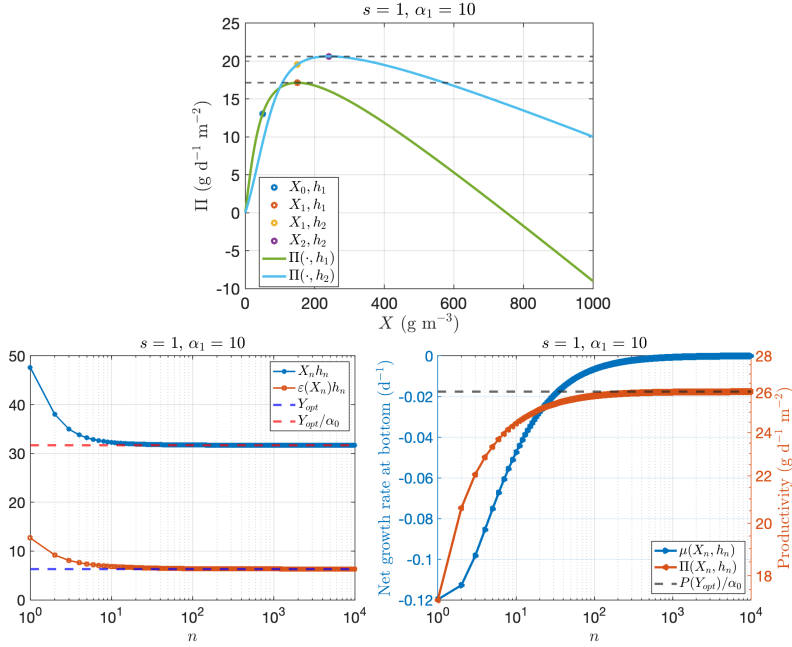


Figure 7: Up: First-two elements of these two sequences. Down Left: Surface biomass $X_n h_n$ and optical depth $\varepsilon(X_n) h_n$ for the sequence $(X_n, h_n)_{n>0}$. Down Right: Productivity $\Pi(X_n, h_n)$ and net growth rate at the reactor bottom $\mu(X_n, h_n) - R$ for the sequence $(X_n, h_n)_{n>0}$.

from the figure on the top, the blue point and the yellow point are the first-two element of the sequence $(X_{n-1}, h_n)_{n>0}$, the red point and the purple point are the first-two element of the sequence $(X_n, h_n)_{n>0}$. Recall that the sequence $(X_{n-1}, h_n)_{n>0}$ always satisfies $\varepsilon(X_{n-1}) h_n = Y_{\text{opt}}$ and the net growth rate at the reactor bottom is always 0. We then only study the asymptotic behaviour of the sequence $(X_n, h_n)_{n>0}$. As shown in bottom left figure, the surface biomass $X_n h_n$ converges to $\frac{Y_{\text{opt}}}{\alpha_0}$ and the optical depth $\varepsilon(X_n) h_n$ converges to Y_{opt} , as proved in Lemma 3.3. The productivity $\Pi(X_n, h_n)$ converges to $P(Y_{\text{opt}})/\alpha_0$, see bottom right figure as proved in Theorem 3.3. Finally, the net growth rate at the reactor bottom converges to zero, which is the global optimum condition in the case where the background turbidity is 0 (see Corollary 3.1). In particular,

since (X_n, h_n) are the optima in the direction of X for each h_n , one can see that the net growth rate at the reactor bottom for these optima are always negative, meaning that the compensation condition is only satisfied asymptotically.

5.3.5 Local optimum in the case $s < 1$

We start with a similar study as in Figure 5 in the case $s < 1$. Recall that the depth of the reactor is given by $h = 0.15$ m and two background turbidity values are given by $\alpha_1 = 0 \text{ m}^{-1}$ and $\alpha_1 = 10 \text{ m}^{-1}$. Figure 8 illustrates the results for $s = 0.365$. Recall that the blue point (X_0, h) satisfies

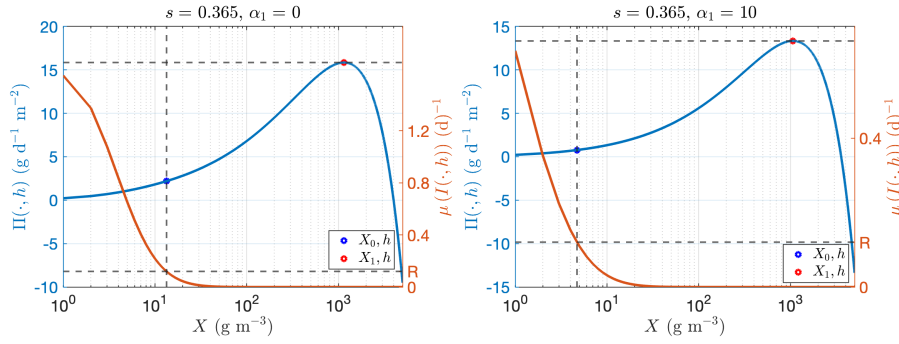


Figure 8: Productivity (Π) with respect to biomass concentration (X) for $h = 0.15$ m. Left: $\alpha_1 = 0 \text{ m}^{-1}$. Right: $\alpha_1 = 10 \text{ m}^{-1}$.

the relation $\varepsilon(X_0)h = Y_{\text{opt}}$ which also means that the net growth rate at the reactor bottom is zero, and the red point (X_1, h) represents the optimum which maximizes the productivity for this depth h . In the case $\alpha_1 = 0 \text{ m}^{-1}$, we find $X_0 = 13.327 \text{ g} \cdot \text{m}^{-3}$ and $X_1 = 1149.298 \text{ g} \cdot \text{m}^{-3}$, whereas we obtain $X_0 = 4.715 \text{ g} \cdot \text{m}^{-3}$ and $X_1 = 1064.574 \text{ g} \cdot \text{m}^{-3}$ in the case $\alpha_1 = 10 \text{ m}^{-1}$. These two points do not coincide even when the background turbidity is zero, which is different from the case $s = 1$.

Figure 9 presents the global behaviour of surface biomass productivity in the case $s = 0.365$. Unlike for the case $s = 1$ (Figure 6), the influence of the background turbidity becomes smaller when $s < 1$. However, similarly to this $s = 1$ case (Right), the productivity becomes larger when the biomass concentration X increases and the water depth h decreases. Furthermore, Figure 10 shows the divergence of the productivity Π , as proved in Theorem 3.3.

5.3.6 Controller test

We present the efficiency of the controller D designed in Proposition 4.1. Let us set $h = 0.1$ m, $s = 1$, $X(0) = [2500, 50] \text{ g m}^{-3}$, $D_{\text{max}} = 10\mu_{\text{max}}$ and keep other parameter settings. Figure 11 illustrates the behaviour of the biomass concentration X under our controller D . Note that the desired biomass concentration $X^* = \text{argmax}_{X \in \mathbb{R}_+} \Pi(X, h)$. One can see that the evolution of the

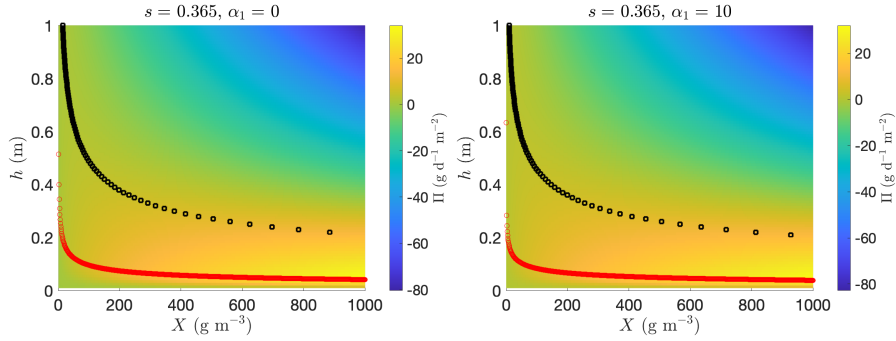


Figure 9: Global behaviour of productivity (Π) with respect to depth (h) and biomass concentration (X). Left: $\alpha_1 = 0 \text{ m}^{-1}$. Right: $\alpha_1 = 10 \text{ m}^{-1}$. The red circles represent the suboptimal couple (X, h) where Π finds its maximum in the direction of h for a given X . The black squares represent the suboptimal couple (X, h) where Π finds its maximum in the direction of X for a given h .

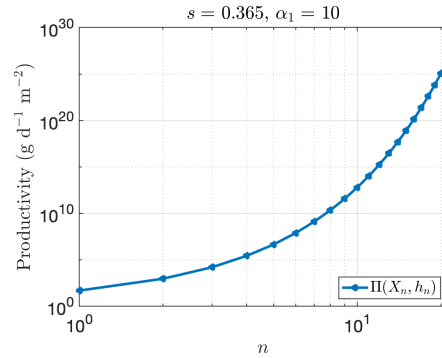


Figure 10: $\Pi(X_n, h_n)$ for the sequence $(X_n, h_n)_{n>0}$.

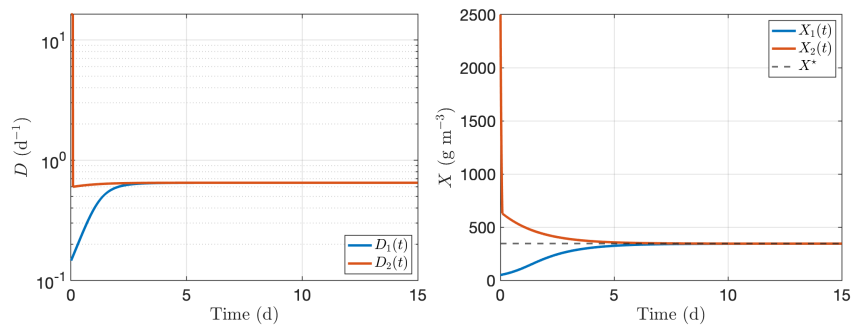


Figure 11: Evolution of the biomass concentration X in closed loop for two initial conditions.

biomass concentration X in closed loop converges to the desired optimal biomass concentration (after five days).

6 Conclusion

The concept of optical productivity P has been defined and a global optimum Y_{opt} has been found to maximize P . This condition corresponds to a situation where the net growth rate at the reactor bottom is zero. This optimum can be used to characterize the optimal water depth which maximizes surface biomass productivity Π for a target biomass concentration value. When the light extinction rate is affine with respect to the biomass concentration, an upper limit to the productivity is given which is obtained for an infinitely small depth and an infinitely large biomass concentration.

The proposed nonlinear controller stabilizes the biomass concentration to its optimal value X^* . It could be improved by integrating an extremum seeking strategy [23, 15] to automatically target the desired biomass without identifying it in advance.

References

- [1] F.G. Acién Fernández, F. García Camacho, and Y. Chisti. Photobioreactors: light regime, mass transfer, and scaleup. In R. Osinga, J. Tramper, J.G. Burgess, and R.H. Wijffels, editors, *Marine Bioprocess Engineering*, volume 35 of *Progress in Industrial Microbiology*, pages 231–247. Elsevier, 1999.
- [2] M. Barceló-Villalobos, P. Fernández-del Olmo, J.L. Guzmán, J.M. Fernández-Sevilla, and F.G. Acién Fernández. Evaluation of photosynthetic light integration by microalgae in a pilot-scale raceway reactor. *Bioresource Technology*, 280:404–411, 2019.
- [3] Q. Béchet, N. Coulombier, C. Vasseur, T. Lasserre, L. Le Dean, and O. Bernard. Full-scale validation of an algal productivity model including nitrogen limitation. *Algal research*, 31:377–386, 2018.
- [4] Q. Béchet, A. Shilton, and B. Guieysse. Modeling the effects of light and temperature on algae growth: state of the art and critical assessment for productivity prediction during outdoor cultivation. *Biotechnology advances*, 31(8):1648–1663, 2013.
- [5] M. Berenguel, F. Rodriguez, F.G. Acién, and J.L. Garcia. Model predictive control of ph in tubular photobioreactors. *Journal of Process Control*, 14(4):377–387, 2004.
- [6] O. Bernard and B. Rémond. Validation of a simple model accounting for light and temperature effect on microalgal growth. *Bioresource Technology*, 123:520–527, 2012.

- [7] N. Broekhuizen, J.B.K. Park, G.B. McBride, and R.J. Craggs. Modification, calibration and verification of the iwa river water quality model to simulate a pilot-scale high rate algal pond. *Water research*, 46(9):2911–2926, 2012.
- [8] F. Casagli, G. Zuccaro, O. Bernard, J.-P. Steyer, and E. Ficara. Alba: A comprehensive growth model to optimize algae-bacteria wastewater treatment in raceway ponds. *Water Research*, 190:116734, 2021.
- [9] J.-F. Cornet and C.-G. Dussap. A simple and reliable formula for assessment of maximum volumetric productivities in photobioreactors. *Biotechnology Progress*, 25(2):424–435, 2009.
- [10] R. De-Luca, F. Bezzo, Q. Bechet, and O. Bernard. Exploiting meteorological forecasts for the optimal operation of algal ponds. *Journal of Process Control*, 55:55–65, 2017.
- [11] D. Demory, C. Combe, P. Hartmann, A. Talec, E. Pruvost, R. Hamouda, F. Souillé, P.-O. Lamare, M.-O. Bristeau, J. Sainte-Marie, S. Rabouille, F. Mairet, A. Sciandra, and O. Bernard. How do microalgae perceive light in a high-rate pond? towards more realistic lagrangian experiments. *The Royal Society*, May 2018.
- [12] M.H.M. Eppink, G. Olivieri, H. Reith, C. van den Berg, M.J. Barbosa, and R.H. Wijffels. From current algae products to future biorefinery practices: a review. In *Biorefineries*, pages 99–123. Springer, 2017.
- [13] J. Grenier, F. Lopes, H. Bonnefond, and O. Bernard. Worldwide perspectives of rotating algal biofilm up-scaling. Submitted paper, 2020.
- [14] E. Molina Grima, J.M. Fernández Sevilla, J.A. Sánchez Pérez, and F. Garcia Camacho. A study on simultaneous photolimitation and photoinhibition in dense microalgal cultures taking into account incident and averaged irradiances. *Journal of Biotechnology*, 45(1):59–69, 1996.
- [15] M. Guay, D. Dochain, and M. Perrier. Adaptive extremum seeking control of continuous stirred tank bioreactors with unknown growth kinetics. *Automatica*, 40(5):881–888, 2004.
- [16] B.-P. Han. A mechanistic model of algal photoinhibition induced by photo-damage to photosystem-ii. *Journal of theoretical biology*, 214(4):519–527, February 2002.
- [17] P. Hartmann, Q. Béchet, and O. Bernard. The effect of photosynthesis time scales on microalgae productivity. *Bioprocess and Biosystems Engineering*, 37(1):17–25, 8 2014.
- [18] Q. Hu, M. Sommerfeld, E. Jarvis, M. Ghirardi, M. Posewitz, M. Seibert, and A. Darzins. Microalgal triacylglycerols as feedstocks for biofuel production: perspectives and advances. *The Plant Journal*, 54(4):621–639, 2008.

- [19] J. Huisman, R.R. Jonker, C. Zonneveld, and F.J. Weissing. Competition for light between phytoplankton species: experimental tests of mechanistic theory. *Ecology*, 80(1):211–222, 1999.
- [20] J. Huisman and F.J. Weissing. Light-limited growth and competition for light in well-mixed aquatic environments: an elementary model. *Ecology*, 75(2):507–520, 1994.
- [21] G.A. Ifrim, M. Titica, G. Cogne, L. Boillereaux, J. Legrand, and S. Carman. Dynamic ph model for autotrophic growth of microalgae in photobioreactor: A tool for monitoring and control purposes. *AIChE Journal*, 60(2):585–599, 2014.
- [22] H.K. Khalil. *Nonlinear Systems*. Pearson, 3 edition, 2002.
- [23] S.-J. Liu and M. Krstic. Introduction to extremum seeking. In *Stochastic Averaging and Stochastic Extremum Seeking*, pages 11–20. Springer, 2012.
- [24] H.-P. Luo and M.H. Al-Dahhan. Analyzing and modeling of photobioreactors by combining first principles of physiology and hydrodynamics. *Biotechnology and bioengineering*, 85(4):382–393, 2004.
- [25] C. Martínez, F. Mairet, and O. Bernard. Theory of turbid microalgae cultures. *Journal of Theoretical Biology*, 456:190–200, November 2018.
- [26] P. Masci, F. Grogard, and O. Bernard. Microalgal biomass surface productivity optimization based on a photobioreactor model. *IFAC Proceedings Volumes*, 43(6):180–185, 2010.
- [27] A. Morel. Optical modeling of the upper ocean in relation to its biogenous matter content (case i waters). *Journal of Geophysical Research: Oceans*, 93(C9):10749–10768, 1988.
- [28] R. Muñoz-Tamayo, F. Mairet, and O. Bernard. Optimizing microalgal production in raceway systems. *Biotechnology progress*, 29(2):543–552, 2013.
- [29] L. Pottier, J. Pruvost, J. Deremetz, J.-F. Cornet, J. Legrand, and C.G. Dussap. A fully predictive model for one-dimensional light attenuation by *chlamydomonas reinhardtii* in a torus photobioreactor. *Biotechnology and Bioengineering*, 91:569–582, 2005.
- [30] S.A. Scott, M.P. Davey, J.S. Dennis, I. Horst, C.J. Howe, D.J. Lea-Smith, and A.G. Smith. Biodiesel from algae: challenges and prospects. *Current Opinion in Biotechnology*, 21(3):277–286, 2010. Energy biotechnology – Environmental biotechnology.
- [31] A. Solimeno, C. Gómez-Serrano, and F.G. Ación. Bio_algae 2: improved model of microalgae and bacteria consortia for wastewater treatment. *Environmental Science and Pollution Research*, 26(25):25855–25868, 2019.

- [32] A. Solimeno, R. Samsó, E. Uggetti, B. Sialve, J.-P. Steyer, A. Gabarró, and J. García. New mechanistic model to simulate microalgae growth. *Algal Research*, 12:350–358, 2015.
- [33] P. Spolaore, C. Joannis-Cassan, E. Duran, and A. Isambert. Commercial applications of microalgae. *Journal of Bioscience and Bioengineering*, 101(2):87–96, 2006.
- [34] H. Takache, G. Christophe, J.-F. Cornet, and J. Pruvost. Experimental and theoretical assessment of maximum productivities for the microalgae *chlamydomonas reinhardtii* in two different geometries of photobioreactors. *Biotechnology progress*, 26(2):431–440, 2010.
- [35] H. Takache, J. Pruvost, and J.-F. Cornet. Kinetic modeling of the photosynthetic growth of *chlamydomonas reinhardtii* in a photobioreactor. *Biotechnology progress*, 28(3):681–692, 2012.
- [36] F.J. Weissing and J. Huisman. Growth and competition in a light gradient. *Journal of theoretical biology*, 168(3):323–336, 1994.
- [37] R.H. Wijffels and M.J. Barbosa. An outlook on microalgal biofuels. *Science*, 329(5993):796–799, 2010.

A Han model to Haldane description

Let us consider the Han model [16]:

$$\begin{cases} \dot{A} = -\sigma IA + \frac{B}{\tau}, \\ \dot{B} = \sigma IA - \frac{B}{\tau} + k_r C - k_d \sigma IB, \\ \dot{C} = -k_r C + k_d \sigma IB, \end{cases} \quad (16)$$

where A, B, C are the relative frequencies of the three possible photosynthetic states of the microalgae which satisfies

$$A + B + C = 1. \quad (17)$$

Here I is the photon flux density, a continuous time-varying signal. The other parameters are σ , that stands for the specific photon absorption, τ which is the turnover rate, k_r which represents the photosystem repair rate and k_d which is the damage rate. The system (16) can be reduced to two equations by using (17). Indeed, one can for instance eliminate B in (16) and gets

$$\begin{cases} \dot{A} = -(\sigma I + \frac{1}{\tau})A + \frac{1-C}{\tau}, \\ \dot{C} = -(k_r + k_d \sigma I)C + k_d \sigma I(1 - A), \end{cases} \quad (18)$$

We then complete the system above with initial conditions

$$(A(0), C(0)) = (A_0, C_0) \in \{(x, y) \in \mathbb{R}_+^2 \mid x + y \in [0, 1]\}.$$

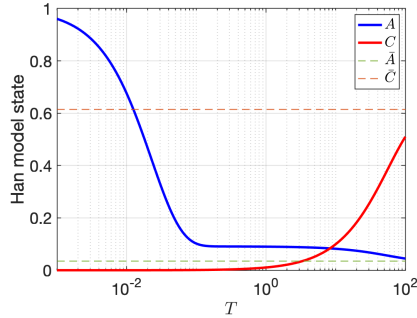


Figure 12: Evolution for open state A and photoinhibition state C with the initial condition $(A(0), C(0)) = (1, 0)$. Note that we use an Euler Explicit scheme to solve the system (18) by using the parameters presented in Table 1. A \log scale is also used for the time variable.

The dynamics of the open state A reaches its steady state following a process whose speed is very high compared to the dynamics of the photoinhibition state C [17] (for instance see Figure 12). This phenomenon is mainly due to the presence of the multiplicative parameter k_d which is relatively small (see Table 1, where an example of possible values for the Han parameters is given). Since we usually focus on light variation at large timescale (larger than second) in real life applications, we can then apply a slow-fast dynamics using singular perturbation theory [22]. More precisely, this consists in equating the first equation of (18) to zero and find the pseudo steady state of A as $\frac{1-C}{\tau\sigma_H I+1}$. Replacing this into the second equation of (18), the previous two equations can finally be reduced to one equation, namely

$$\dot{C} = -(k_d\tau \frac{(\sigma I)^2}{\tau\sigma I+1} + k_r)C + k_d\tau \frac{(\sigma I)^2}{\tau\sigma I+1}.$$

The growth rate in the steady state of this system is then defined by

$$\mu_{\text{Han}}(I) := \frac{k\sigma I}{\frac{k_d}{k_r}\tau(\sigma I)^2 + \tau\sigma I + 1}. \quad (19)$$

Finally by identifying (1) and (19) correctly, one finds

$$\theta = k\sigma, \quad I^* = \sqrt{\frac{k_r}{k_d\tau\sigma^2}}, \quad \mu_{\text{max}} = \frac{k\sigma}{\tau\sigma + 2\sqrt{\frac{k_d\tau\sigma^2}{k_r}}}. \quad (20)$$

B Explicit computations for average growth rate

In this section, we provide details about the computation on $\bar{\mu}$. As mentioned in Appendix A, the growth rate described by Han model can be easily written in

the Haldane description. We choose to present the corresponding computation hereafter with Han model parameters. From the definition of $\bar{\mu}$ (4), one has

$$\bar{\mu} = \frac{1}{h} \int_{-h}^0 \mu_{\text{Han}}(I(X, z)) dz = \frac{k_r k \sigma}{h \varepsilon(X)} \int_{I_b}^{I_s} \frac{1}{k_d \tau (\sigma I)^2 + k_r (\tau \sigma I + 1)} dI,$$

where $I_b = I_s \exp(-\varepsilon(X)h)$. Define $a = k_d \tau \sigma^2$, $b = k_r \tau \sigma$, $c = k_r$. According to the sign of the discriminant Δ of equation $aI^2 + bI + c$, three cases must be considered.

- $\Delta > 0$: Then there exists two reel roots denoted by $d_1 = \frac{-b + \sqrt{b^2 - 4ac}}{2a}$ and $d_2 = \frac{-b - \sqrt{b^2 - 4ac}}{2a}$. Hence one has

$$\bar{\mu} = \frac{k_r k \sigma}{ah \varepsilon(X)} \left(e_1 \ln \left| \frac{I_s - d_1}{I_b - d_1} \right| + e_2 \ln \left| \frac{I_s - d_2}{I_b - d_2} \right| \right).$$

with $e_1 + e_2 = 0$ and $e_1 d_2 + e_2 d_1 = -1$, i.e. $e_1 = \frac{1}{d_1 - d_2} = \frac{a}{\sqrt{b^2 - 4ac}}$ and $e_2 = \frac{1}{d_2 - d_1} = -\frac{a}{\sqrt{b^2 - 4ac}}$. Using $e_2 = -e_1$, we find

$$\bar{\mu} = \frac{k_r k \sigma e_1}{ah \varepsilon(X)} \ln \left| \frac{(I_s - d_1)(I_b - d_2)}{(I_b - d_1)(I_s - d_2)} \right|.$$

- $\Delta = 0$: Then there exists a unique root denoted by $d = -\frac{b}{2a}$. And one has

$$\bar{\mu} = \frac{k_r k \sigma}{h \varepsilon(X)} \frac{I_s - I_b}{(I_s - d)(I_b - d)}$$

- $\Delta < 0$: Then one has

$$aI^2 + bI + c = \frac{4ac - b^2}{4a} \left(\left(\frac{I + \frac{b}{2a}}{\sqrt{\frac{4ac - b^2}{4a^2}}} \right)^2 + 1 \right).$$

Applying a change of variable by setting $y = \frac{I + \frac{b}{2a}}{\sqrt{\frac{4ac - b^2}{4a^2}}}$, one gets

$$\bar{\mu} = \frac{k_r k \sigma}{h \varepsilon(X)} \frac{2}{\sqrt{4ac - b^2}} \left(\arctan\left(\frac{2aI_s + b}{\sqrt{4ac - b^2}}\right) - \arctan\left(\frac{2aI_b + b}{\sqrt{4ac - b^2}}\right) \right).$$

Since one has the explicit formulation of the average growth rate $\bar{\mu}$, the surface biomass concentration Π can be then computed explicitly including its derivatives. This is at the basis of the determination of the optimal biomass concentration X for a given depth h .